

Detailed Imager Evaluation and Unique Applications of a New 20cm x 25 cm Size Mercuric Iodide Thick Film X-Ray Detector

G. Zentai, L. Partain, R. Pavlyuchkova, C. Proano and G. Virshup

Varian Medical Systems, Mountain View, CA 94043 USA

B. N. Breen, A. Vilensky, O. Dagan, E. Meerson, M. Shieber and H. Gilboa

Real Time Radiography Readout, Jerusalem Technology Park, Jerusalem 91487 Israel

J. Thomas

Uniformed Services University, Bethesda, MD 20814 USA

ABSTRACT

We previously reported on 2" x 2" and 4" x 4" size imagers, direct digital radiography X-ray detectors, based on photoconductive polycrystalline mercuric iodide deposited on a flat panel thin film transistor (TFT) array, as having great potential for use in medical imaging, NDE, and security applications. Recently we successfully upgraded our mercuric iodide deposition technique to 20 cm x 25 cm size, the size required in common NDE and security imaging applications. A TFT array with a pixel pitch of 127 microns was used for this imager. The mercuric iodide direct conversion layers were vacuum deposited onto TFT array by Physical Vapor Deposition (PVD).

In addition to successful imager scale up, more sophisticated, non-TFT based detectors were developed in order to improve analysis methods of the mercuric iodide photoconductor. Measurements on mercuric iodide photoconductor were performed using a 36 x 6 electrode array on a 10cm x 10cm substrate (total of 216 measurement points). The array is formed by 36 palladium stripes on the glass substrate, upon which the mercuric iodide is deposited, and 6 palladium stripes that are deposited on top of the mercuric iodide layer. These two sets of electrodes are oriented at 90 degrees to each other to create the measurement matrix. These detectors were evaluated in radiographic mode, continuous fluoroscopic mode and pulsed fluoroscopic mode. Mercuric iodide coatings with thickness ranging between 140 microns and 300 microns were tested using beams with energies between 40 kVp and 100 kVp utilizing exposure ranges typical for both fluoroscopic and radiographic imaging.

Diagnostic quality radiographic and fluoroscopic images at up to 15 pulses per second were demonstrated. We evaluated the dark current, sensitivity and MTF characteristics. The MTF is determined primarily by the aperture and pitch of the TFT array with Nyquist frequency of $\sim 3.93 \text{ mm}^{-1}$ (127 micron pixel pitch). The MTF curve of a good quality HgI_2 imager is very close to the theoretical sinc function. Image lag characteristics of mercuric iodide appear adequate for fluoroscopic rates.

Keywords: imaging, X-ray radiology, polycrystalline, mercuric iodide, imaging detectors, flat-panel imaging arrays, mercuric iodide X-ray imager.

1. INTRODUCTION

Direct detector materials must exhibit several attributes including high x-ray absorption, high charge collection efficiency, low dark current and good uniformity. These are difficult to achieve in a single material. Nevertheless because blurring due to spreading of light is eliminated, higher resolutions are possible with direct detectors than with detectors utilizing phosphor coatings.

This paper describes measurements performed on high-resolution image sensors using HgI_2 photoconducting layers in the direct detection mode of operation.

	Poly-HgI₂	a-Se	Comments
Atomic Number (Z)	80, 53	34	Absorption increases with Z
Energy Band Gap (E _g) eV	2.1	2.2	Wide gap reduces dark current
Charge Pair Formation Energy (W), eV	5.5	42	Lower W increases the gain
Mobility Life-time Product ($\mu\tau$) cm ² /V	1.5x10 ⁻⁵	10 ⁻⁶ – 10 ⁻⁵	Higher $\mu\tau$ improves the charge collection
Operational Electric Field (E) V/micron	0.5-1	10	Lower E reduces electrical breakdown
Processing Temperature (°C)	100	400	Lower temperature – simpler process

Table 1. Comparison of amorphous Se and poly HgI₂

Polycrystalline semiconductor HgI₂ films directly convert X-rays into electrical signals with high efficiency, which is advantageous for digital radiography X-ray detectors¹⁻¹³. Table 1 summarizes film properties of amorphous Se and polycrystalline HgI₂, two of the materials considered for fluoroscopic direct imaging.

The high Z value of HgI₂ indicates that it is an efficient material for absorbing X-rays for clinically used X-ray exposure energies. In addition, the X-ray energy required to generate an electron-hole pair in mercuric iodide photoconductor, as designated by the parameter W, is relatively low. The lower the W, the higher the number of charges generated by X-ray photons, and so the higher the X-ray sensitivity. As Table 1 shows, the parameter W is smaller for HgI₂ compared to Se by a factor of 7.

The larger the mobility-lifetime ($\mu\tau$) product of the charge carriers, the greater the distance the electrical charges move in the detector. Greater distances result in higher sensitivity due to better charge collection. The high Z number, low W and high $\mu\tau$ -product result in very high signal, which can overcome all noise sources in fluoroscopic modes of operation. The ability to operate the HgI₂ imager at low bias voltages, gives a further advantage; we can use low voltage electronic design.

Mercuric iodide is processed at very low temperature. This allows simple manufacturing techniques, a greater choice of substrate materials, and less danger of damaging the expensive TFTs during the coating process. Low manufacturing temperature will also permit the use of TFTs deposited on plastic substrates, when they become available in the future. Plastic substrates offer cost-effective parts that lack brittleness and fragility, characteristics of currently used glass substrates. The temperature stability of HgI₂ allows operation, storage and transportation of these imagers under regular conditions and temperatures. Other materials, such as amorphous selenium, have storage and transportation problems that require them to be shipped and stored under special conditions. Even at non-extreme temperatures, amorphous selenium can irreversibly recrystallize with time, ceasing to act as a detector.

2. SAMPLE PREPARATION

2.1 Photoconductor Deposition

HgI₂ material deposition technique on small area substrates has been published earlier¹. For the first time, a full-scale 20x25cm imager has been manufactured using mercuric iodide photoconductor. Manufacture of such imagers required scale-up of the small reactors that have been used until now for production of 5cm x 5cm and 10cm x 10cm imagers. The substrates of the larger imagers are TFT arrays with 127 μ m x 127 μ m pixel size, 10cm x 10cm (768x768 pixels) and 20cm x 25cm (1536x1920 pixels) active area.

The reactor is based upon a 25" (63cm) diameter stainless steel vacuum vessel. Highly purified mercuric iodide powder is loaded into evaporators in the base of the reactor. The TFT array is suspended over the evaporators. By proper choice of evaporator temperature and array temperature, a highly oriented (c-axis) and dense layer of polycrystalline mercuric iodide is deposited on the TFT array. This reactor has been used to deposit polycrystalline mercuric iodide layers in a thickness range of 40 μ m to >300 μ m.

After deposition of the mercuric iodide photoconductor, a bias electrode is deposited on top of the film followed by a polymer encapsulation layer.

3. EXPERIMENTAL RESULTS ON NON-TFT BASED PHOTOCONDUCTOR SAMPLES

3.1 Striped Electrode Detector and Measuring System

Measurements on mercuric iodide photoconductor were performed using a 36 x 6 electrode array on a 10cm x 10cm substrate (total of 216 measurement points). The array is formed by 36 palladium stripes on the glass substrate, upon which the mercuric iodide is deposited, and 6 palladium stripes that are deposited on top of the mercuric iodide layer. These two sets of electrodes are oriented at 90 degrees to each other to create the measurement matrix. Schematics of the part of this substrate and the measurement system is presented in Figure 1.

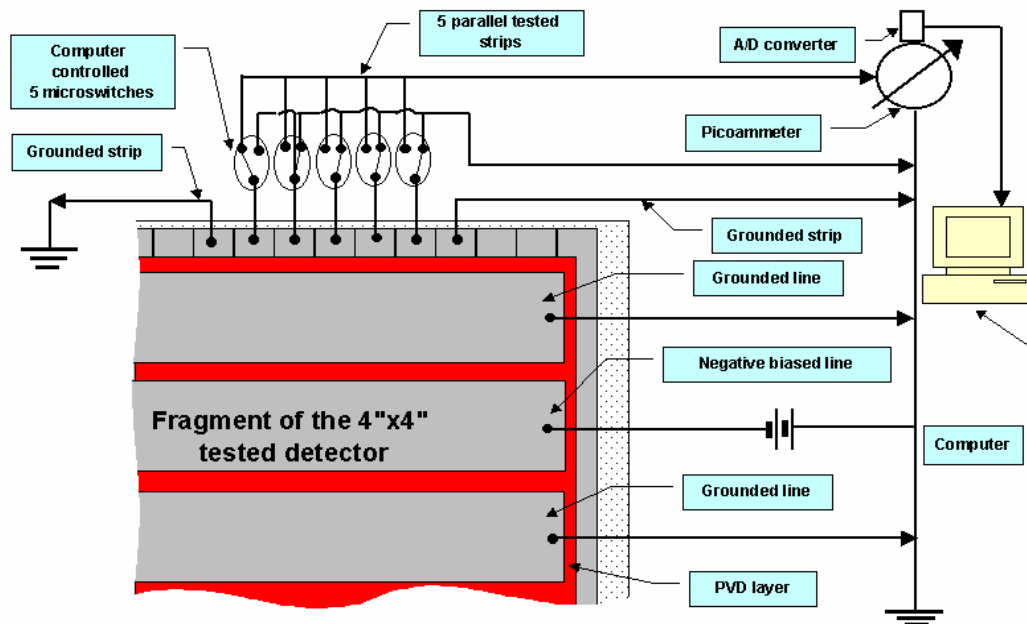


Figure 1. Schematic of striped electrode detector and measuring system

Figure 2 presents typical photoconductor sensitivity results obtained using this characterization technique. Significant data on signal uniformity is obtained by this technique, without the need to use expensive TFT arrays for basic photoconductor characterization. The sensitivity looks uniform on the whole area within $\pm 15\%$.

3.2 Characterization of Mercuric Iodide Photoconductor as a Function of X-Ray Energy

Measurements were carried out on two basic parameters of the mercuric iodide photoconductor: Sensitivity as a function of photon energy and response linearity as a function of photon flux. Data was acquired under various conditions of X-ray generator voltage (kVp), generator current and added filtration which hardens the X-ray spectrum for a given generator voltage.

Figure 3 presents response of a mercuric iodide detector as a function of X-ray generator voltage and of bias on the detector layer. Detector response is nearly independent of X-ray photon energy at X-ray voltages between 50kVp and 100kVp. The data on signal linearity as a function of exposure rate was published previously¹⁹.

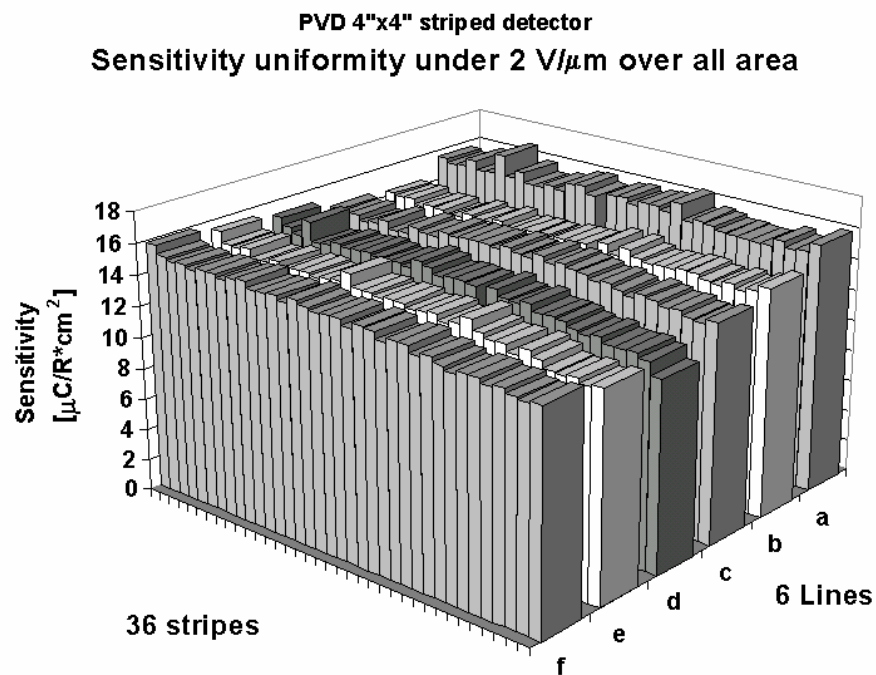


Figure 2: Response uniformity of a mercuric iodide detector composed of palladium stripe electrodes

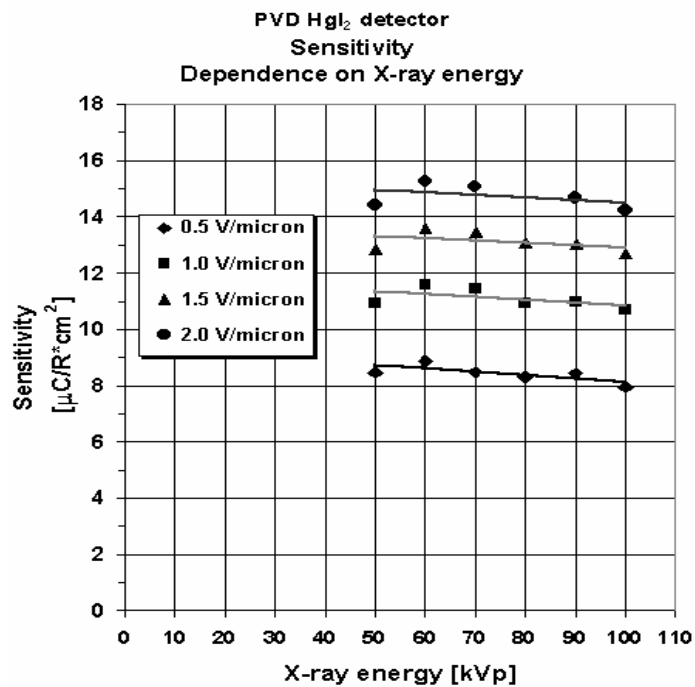


Figure 3: Response of a 300 micron thick mercuric iodide detector as a function of X-ray energy with added 2mm Al filtration

4. CHARACTERIZATION OF HgI₂ IMAGERS

We measured and evaluated the most important parameters of HgI₂ X-ray imagers. The parameters included are the dark current, sensitivity at a given X-ray energy, image lag, and MTF. In addition, radiographs of different small objects were produced to test the imaging performance.

4.1. Dark Current

The dark current of HgI₂ imagers generally increases superlinearly with the applied bias voltage. Typical dark current values for HgI₂ imagers are given in Fig. 4. The dark current at 1V/μm electrical field is about 600pA/mm² for the large imager (HgI₂ #22, 20cm x 25cm area). This value is about twice as high as was measured, about a year ago, on imager #10 (10cm x 10cm size). One of the most recent 10cm x 10cm size imagers (HgI₂ #21) has much lower dark current, ~130pA/mm² at the same 1V/μm relative bias, which indicates that this value should also be obtainable for the larger imager by improving the deposition method in the new large PVD system. We have been working on modified deposition process parameters to improve this value further and have already some other deposition technique where we observed less than 10pA/mm² dark current at 0.5V/μm relative bias on small samples¹⁴.

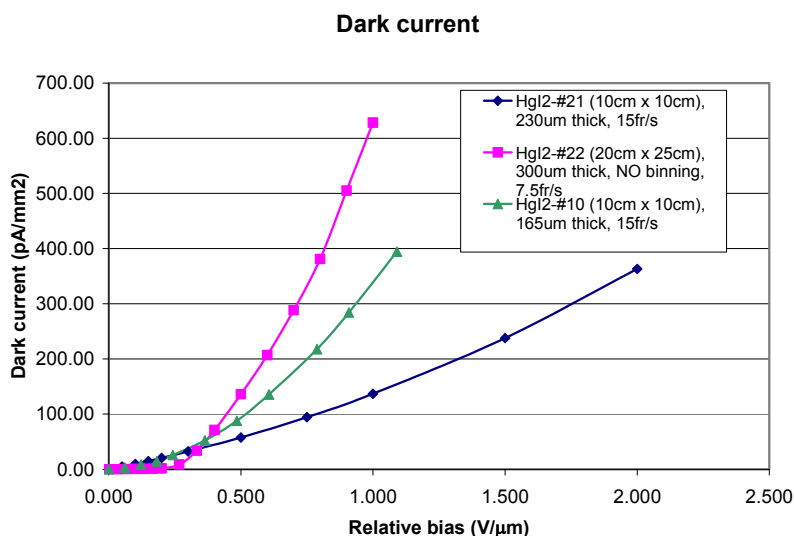


Fig. 4. Dark current of typical PVD-HgI₂ 10 cm x 10 cm size imagers and of a new 20cm x 25 cm size imager.

4.2. Sensitivity

Most of the sensitivity measurements were taken at 60kVp x-ray energy with 0.1mm Cu filtering. The imagers were tested in continuous fluoroscopic mode mostly at 15fr/s frame rate except for the 20cm x 25cm size imager in non-binning mode where the frame rate was 7.5fr/s. (We can run this imager up to 30 fr/s rate when we bin the pixels 2x2). The sensitivity data presented here are absolute values and are not corrected for the absorption of the imagers. The sensitivity of some of the imagers is close to 10μC/cm²/R at 1V/μm electrical field (Fig. 5). This value is about three times higher than the best value measured on a 600μm thick CsI₂ indirect type imager of 3.3 μC/R/cm² at the same energy (Varian internal data). It is also very promising that the sensitivity of the new 20cm x 25cm size new imager is high and it is in the same range as the sensitivity of some smaller (e.g. HgI₂ #10, 10cm x 10cm size) imagers.

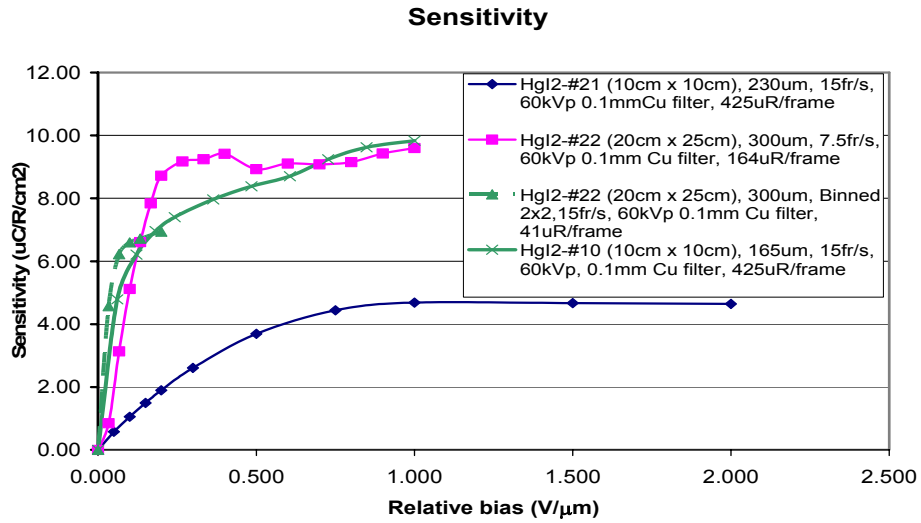


Fig. 5. Sensitivity of some HgI₂ imagers including the new 20 cm x 25 cm size imager

4.3. Homogeneity of the Sensitivity

We measured the pixel-to pixel inhomogeneity of the sensitivity on imager #21 and #22 (Fig. 6). The values plotted are the standard deviation of the sensitivity relative to the average sensitivity (relative standard deviation of sensitivity). This is a good measure of the inhomogeneity because if this value is high, that means, we have larger scattering in the sensitivity value from pixel to pixel.

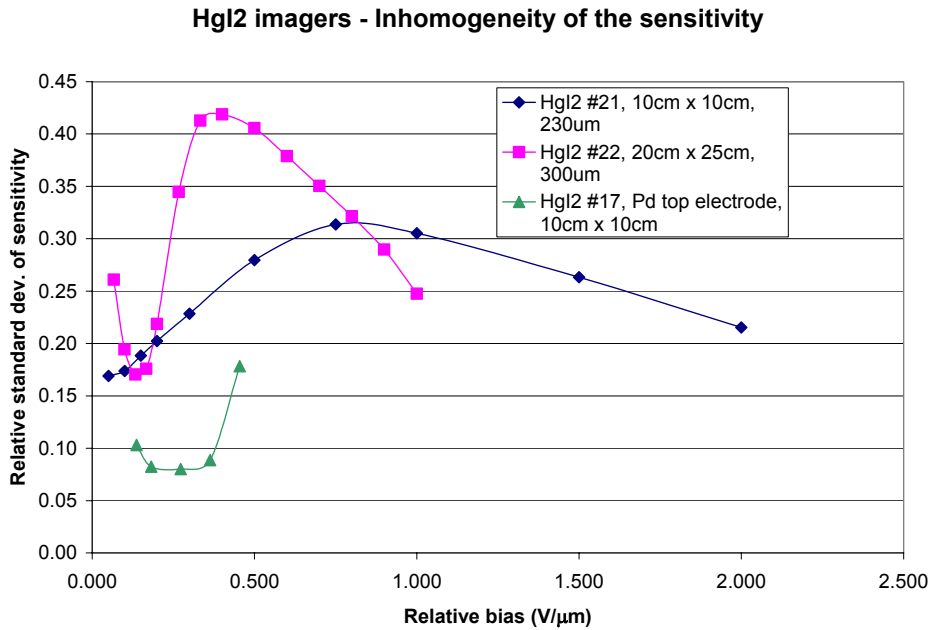


Fig. 6. Pixel to pixel inhomogeneity of the sensitivity

We can correct the pixel to pixel variation with a gain correction method (normalizing all pixel sensitivity to the average value). However if the gain variation is too high this method always increases the noise, mostly the so called fix pattern noise because the same pixels have always slightly higher or lower values than the average. This is different from the random noise where the pixel values randomly vary around the average value but still degrades the imager properties such as the DQE value. As we can see from Fig. 6 the standard deviation of the sensitivity depends on the bias voltage and for imager #21 and #22 varies between 16% and 44% (0.16-0.44). From other imaging experiments we know that this value should be less than 10% (0.1) to get optimum performance of the imager.

An earlier imager (#17) already had the required homogeneity as it has a bias range where the standard deviation of sensitivity is less than 10% (0.1). Fig. 7 demonstrates how this homogeneity (or inhomogeneity) shows up on the sensitivity (gain) distribution. From this Figure it is clear that imager #17 has a much narrower signal (gain) distribution than imagers #21 or #22 during a homogeneous x-ray illumination. Fig. 8 indicates that the narrow (9%) distribution can easily be corrected to better than 2% by the “VIVA” software, developed by Varian Medical Systems. However these Figures also reveal that the large area deposition system should be further improved to get similar results obtained on the smaller #17 array.

Imager #17, #21 and #22 flat field uniformity

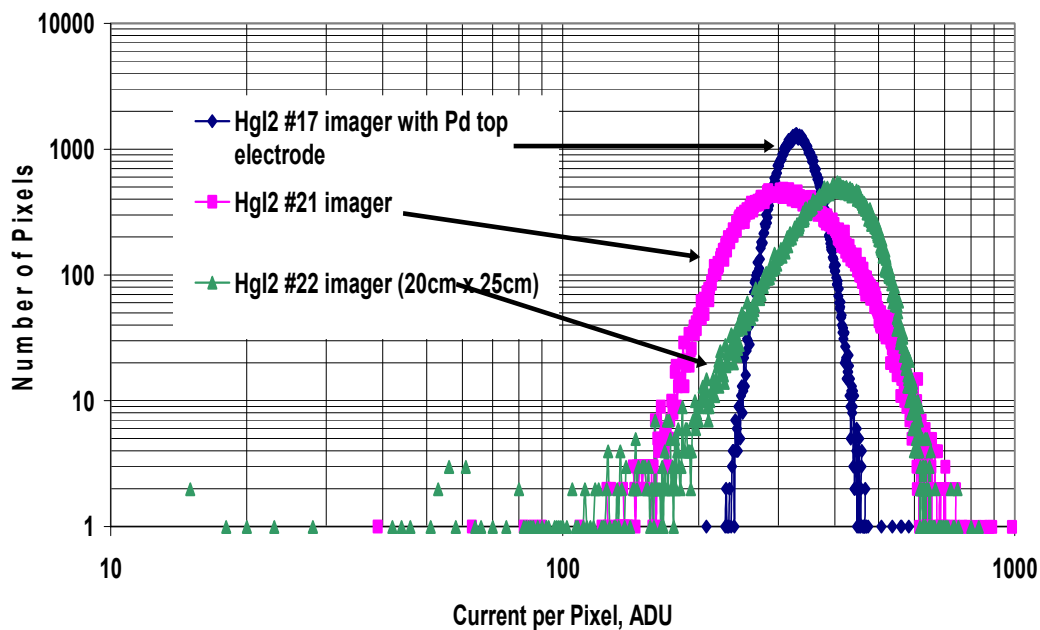


Fig. 7. Flatfield uniformity (distribution of the signal level at a homogeneous x-ray illumination). Narrower distribution results in better image quality

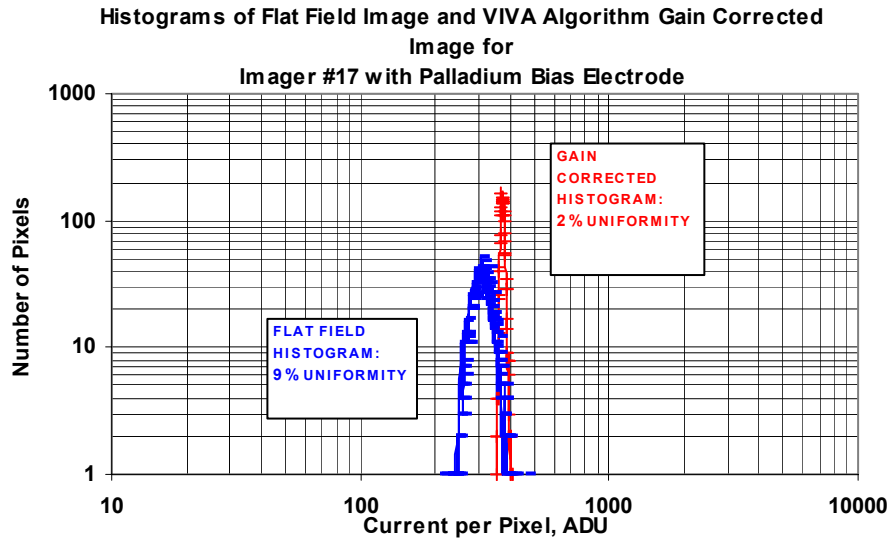


Fig. 8. Narrow distribution of the gain can be easily corrected by the Varian “VIVA” software.

4.3. Image Lag

The image lag was checked in pulsed fluoro mode by using 3ms x-ray pulses at 15fr/s rate (Fig. 9). A continuous series of x-ray pulses was applied for a minimum of 30s. The average exposure was $150\mu\text{R}/\text{frame}$. Signal decay was measured immediately following the exposure series. The first frame image lag is less than 10% of the signal at $0.4\text{V}/\mu\text{m}$ bias and decreases further to less than 8% by increasing the bias to $0.8\text{V}/\mu\text{m}$. After the first frame the residual signal drops gradually reaching about 1% at the 15th frame (after 1s).

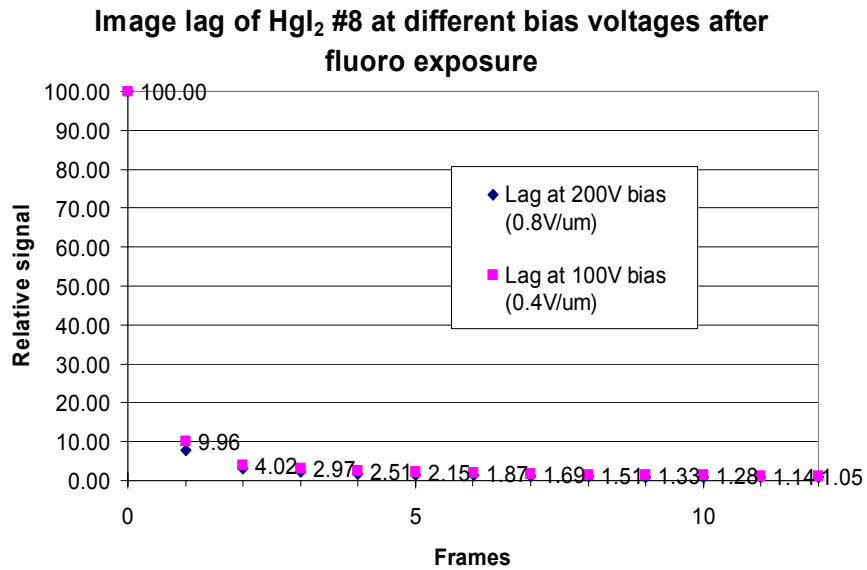


Fig. 9. Image lag as a function of bias voltage (HgI_2)

4.4. Resolution

One of the best measures for the resolution of an imager system is the Modulation Transfer Function. This function gives the output/input transfer ratio of a sine wave as a function of spatial frequency. By definition the zero frequency transfer ratio is 1.

The MTF of a 10cm x 10cm size imager with 230 μ m thick HgI₂ and of the new 20cm x 25cm imager with 300 μ m thick HgI₂ layer was measured by the slit method with 2 pieces of 4mm thick Ta sheets. 50 μ m slit was arranged between the Ta sheets. The x-ray energy was 70kVp with an added 0.1mm Cu filter. The angle of the slit to the pixels was $\sim 2^\circ$. The 50 μ m slit width gave about 6% error at 127 μ m pixels at the Nyquist frequency, which was corrected in the final data (Fig. 10).

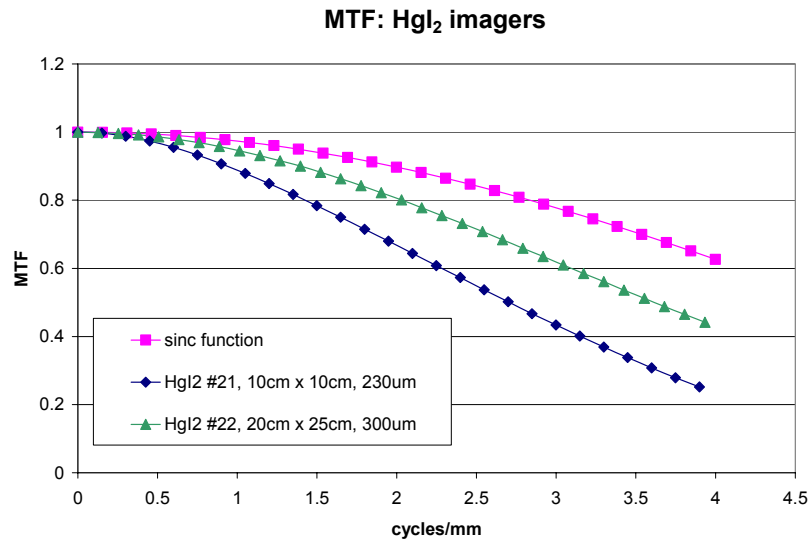


Fig. 10. MTF of HgI₂ imagers #21 (10cm x 10cm) and #22 (20cm x 25cm) compared to the theoretical sinc function

Though the thickness of the smaller #21 imager is only 230 μ m, its MTF is lower than that of the #22 imager with thicker (300 μ m) HgI₂ layer. This shows that the MTF is probably does not degrade with the thickness and the most probable cause of the lower than expected MTF of #21 imager is that the size of the HgI₂ crystallites are too large. We observed similar effect earlier on other HgI₂ imagers. If the size of the HgI₂ crystallites are comparable to the pixel size, than the resolution (MTF) significantly degrades because the large crystallites overlap more than one pixel; so the charges generated in a crystallite are shared between neighboring pixels. However, it is promising that the thicker array has better MTF.

5. IMAGING WITH HgI₂ ARRAYS

A few sample NDE images are shown in Figs. 11-13. For X-ray imaging we used a Hamamatsu microfocus tube (10 μ m focal spot) working at 130kVp and 97 μ A. The imager were running at 15fr/s. The source-detector distance was about 1m and the source-target distance was varied to get different image magnification. Fig. 11 is the X-ray image of an electronic wristwatch with analog display. The battery is the large black object at the bottom of the image. At top-left side the quartz crystal is visible with the wires soldered.

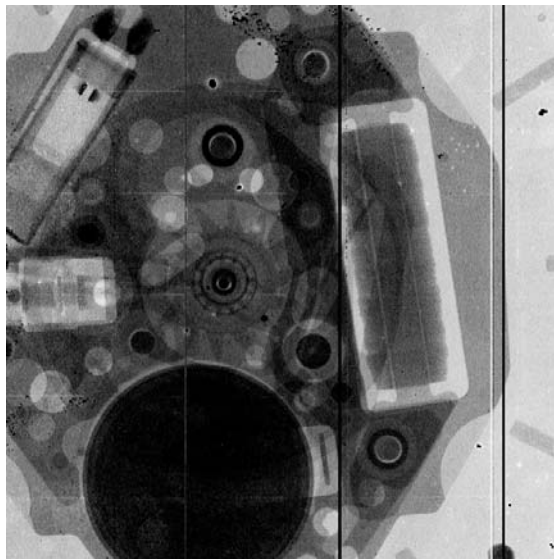


Fig. 11. Electronic wristwatch with analog display (~5X magnification)

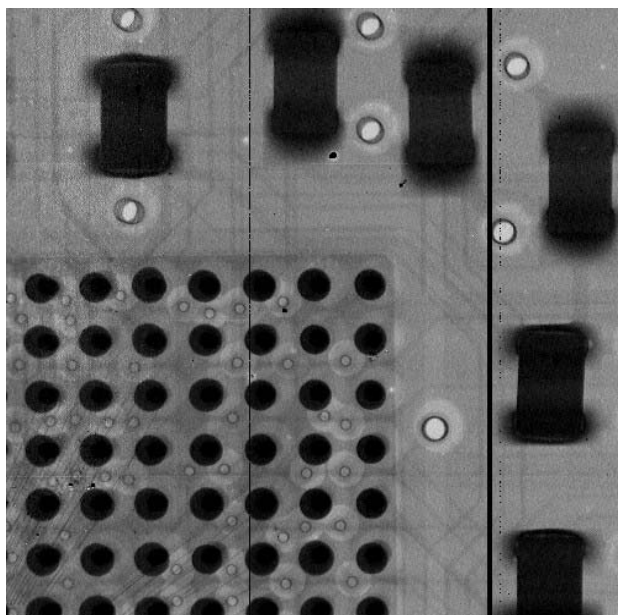


Fig. 12. BGA bonding of an FPGA circuit (~10X magnification)

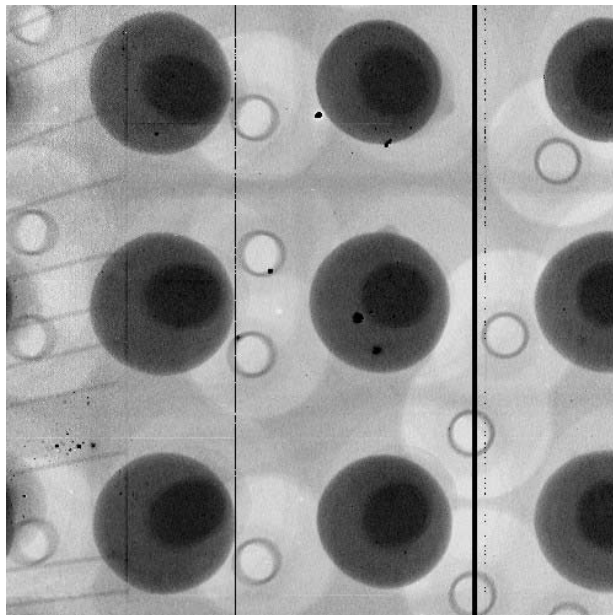


Fig. 13. An enlarged part of the previous picture – some of the soldering balls are slightly misplaced (~40X)

Fig. 12 and 13 show how a BGA (Ball Grid Array) bonded multipin FPGA is attached to the PCB board. While in Fig. 12 the positioning and the attachment of the FPGA looks OK but at larger magnification (Fig. 13) it is visible that some of the soldering balls were slightly misplaced (darker dots are not always in the middle of the balls). This kind of tests of electronic circuits is very important to predict and avoid later failures especially at critical (military, space, medical) applications. These images prove the very high spatial resolution and sensitivity capacity of the HgI₂ material.

6. SUMMARY

Images obtained with 10cm x 10cm and 20cm x 25cm imaging pixilated arrays using PVD-HgI₂ films are shown. Data is also presented of measurements performed on mercuric iodide photoconductor detectors based upon striped electrodes (non-TFT). HgI₂ arrays demonstrate high sensitivity to x-rays and excellent spatial resolution. The low image lag of the HgI₂ detectors opens new applications for this material, especially those requiring extreme sensitivity such as fluoroscopy, which is beyond the capabilities of the existing thin film detectors. The pixel-to-pixel gain homogeneity needs to be improved on the large array at least to that level as seen in the smaller imager #17 and make the deposition process reproducible to optimize the imaging properties of the HgI₂ material. Further reduction in dark current is necessary to apply this material for long exposure applications (radiographic imaging); however the high spatial resolution, which is comparable to that of a-Se, and the higher sensitivity and temperature stability than that of a-Se make this material a good candidate for those uses. High resolution images demonstrate the applicability of x-ray imaging technique for manufacturing, quality testing and other NDE and security applications.

7. ACKNOWLEDGEMENTS

The authors are grateful to the members of the RTR Testing group, I. Baydjanov and M. Kaminsky for carrying out the X-ray response linearity testing and Chris Webb from Varian for helping with the MTF measurements and evaluation.

This work was supported by grant number MDA905-02-1-0012 from the Navy Bureau of Medicine and Surgery and managed by the Henry M. Jackson Foundation for the Advancement of Military Medicine.

8. REFERENCES

1. M. Schieber, H. Hermon, A. Zuck, A. Vilensky, L. Melekhov, R. Shatunovsky, E. Meerson and Y. Saado, *Polycrystalline Mercuric Iodide Detectors*, Proc. of the SPIE on Medical Applications, Vol. 3770 (1999) 146.
2. M. Schieber, H. Hermon, R.A. Street, S.E. Ready, A. Zuck, A. Vilensky, L. Melekhov, R. Shatunovsky, M. Lukach, E. Meerson, Y. Saado and E. Pinhasy, *Mercuric Iodide Thick Films for Radiological X-ray Detectors*, Proc. of the SPIE Vol. 4142 (2000) 197.
3. M. Schieber, H. Hermon, R. Street, S. Ready, A. Zuck, A. Vilensky, L. Melekhov, R. Shatunovsky, E. Meerson, Y. Saado, *Radiological X-ray Response of Polycrystalline Mercuric Iodide Detectors*, Proc. of the SPIE on Medical Imaging 2000 San Diego, Vol. 3977 (2000) 48.
4. H. Hermon, M. Schieber, M. Goorsky, T. Lam, E. Meerson, H. Yao, J. Erickson, and R.B. James, *Characterization of CZT Detectors Grown From Horizontal and Vertical Bridgman*, Proc. of the SPIE on Hard X-ray and Gamma-ray Radiation, Vol. 4141 (2000) 186.
5. M. Schieber, H. Hermon, A. Zuck, A. Vilensky, L. Melekhov, R. Shatunovsky, E. Meerson, H. Saado, *Theoretical and experimental sensitivity to X-rays of single and polycrystalline HgI₂ compared with different single crystal detectors*, NIMA Vol. 458 (2001) 41.
6. M. Schieber, R. B. James, H. Hermon, A. Vilensky, I. Baydjanov, M. Goorsky, T. Lam, E. Meerson, H.W. Yao, J. Erickson, E. Cross, A. Burger, J.O. Ndap, G. Wright, and M. Fiederle, *Comparison of Cadmium Zinc Telluride Crystals Grown by Horizontal and Vertical Bridgman and From the Vapor Phase*, Accepted for publication in JCG (2001).

7. M. Schieber, H. Hermon, A. Zuck, A. Vilensky, L. Melekhov, R. Shatunovsky, E. Meerson, Y. Saado, M. Lukach, E. Pinhasy, S.E. Ready, and R.A. Street, *Thick Films of X-Ray Polycrystalline Mercuric Iodide Detectors*, Journal of Crystal Growth, 225 (2-4) (2001) 118.
8. H. Hermon, M. Schieber, A. Zuck, A. Vilensky, L. Melekhov, E. Shtekel, A. Green, O. Dagan, S.E. Ready, R.A. Street, G. Zentai, and L. Partain, *Deposition of Thick Films of Polycrystalline Mercuric Iodide X-Ray Detectors*, Proc. of the SPIE, MI 2001 – Vol. 4320 (2001) 133.
9. R. A. Street, M. Mulato, S. E. Ready, R. Lau, J. Ho, K. Van Schuylenbergh, M. Schieber, H. Hermon, A. Zuck, A. Vilensky, K. Shah, P. Bennett and Y. Dmitryev, *Comparative Study of PbI₂ and HgI₂ as Direct Detector Materials for High Resolution X-ray Image Sensors*, Proc. of the SPIE MI 2001 - Vol. 4320 (2001) 1.
10. M. Schieber, H. Hermon, A. Zuck, A. Vilensky, L. Melekhov, M. Lukach, E. Meerson, Y. Saado, E. Shtekel, B. Reisman, G. Zentai, E. Seppi, R. Pavlyuchkova, G. Virshup, L. Partain, R. Street, S. E. Ready and R. James, *Non Destructive Imaging with Mercuric Iodide Thick Film X ray detectors*, Proc. of the SPIE NDE 2001 - Vol. 4335 (2001) 43.
11. R.A. Street, S. E. Ready, L. Melekhov, J. Ho, A. Zuck and B. Breen. *Approaching the Theoretical X-ray Sensitivity with HgI₂ Direct Detection Image Sensors*, Proc. of the SPIE MI 2002 –Vol. 4682 (2002) 414.
12. G. Zentai, L. Partain, R. Pavlyuchkova, G. Virshup, A. Zuck, L. Melekhov, O. Dagan, A. Vilensky and H. Gilboa, *Large Area Mercuric Iodide X-Ray Imager*, Proc. of the SPIE MI 2002 – Vol. 4682 (2002) 592.
13. G. Zentai, L. Partain, R. Pavlyuchkova, C. Proano, G. Virshup, B. N. Breen, A. Zuck, B. Reisman, A. Taieb and M. Schieber, *Large area mercuric iodide thick film X-ray detectors for fluoroscopic (on-line) imaging*, Proc. of the SPIE-NDE 2002 – Vol. 4702 (2002) 446.
14. A. Street, S. E. Ready, K.V. Schuylenbergh, J. Ho, J. B. Boyce, P. Nylén, K. Shah, L. Melekhov and H. Hermon *Comparison of PbI₂ and HgI₂ for Direct Detection Active Matrix X-Ray Image Sensor*, J. App. Phys. Vol 91 (2002), No. 5, 3345.
15. R. A. Street, *Technology and Applications of Amorphous Silicon*, Springer, 1999. ed., J. M. Boone, J. A. Seibert, Med. Phys. 24 (1997), 1661.
16. J. H. Hubbell, S. M. Seltzer, <http://physics.nist.gov/PhysRefData/XrayMassCoef/cover.html>, (NIST public domain).
17. I. A. Cunningham in (J. Beutel, H. L. Kundel, R. L. Van Metter, eds.), *Handbook of Medical Imaging, Vol 1*, SPIE Press 2000.
18. W. Zhao, J. A. Rowlands, *X-Ray Imaging Using Amorphous Selenium: Feasibility of a Flat Panel Self- Scanned Detector for Digital Radiology*, Med. Phys. 22 (1995), 1595.
19. G. Zentai, L. Partain, R. Pavlyuchkova, C. Proano and G. Virshup, L. Melekhov, A. Zuck, B. N. Breen, O. Dagan, A. Vilensky, M. Schieber and H. Gilboa, P. Bennet, K. Shah and Y. Dmitriev, J. Thomas, M. Yaffe and D. Hunter, *Mercuric Iodide and Lead Iodide X-Ray Detectors for Radiographic and Fluoroscopic Medical Imaging*, to be published in Proc. of the SPIE MI 2003 – Vol. 5030 (2003).